AGU ADVANCING EARTH AND SPACE SCIENCES

Geophysical Research Letters

RESEARCH LETTER
10.1029/2024GL111092

Ice Thickness-Induced Variations in Effective Pressure and Basal Conditions Influence Seasonal and Multi-Annual Ice Velocity at Sermeq Kujalleq (Jakobshavn Isbræ)

Xi Lu[1,2,3], Andrew Sole[3], Stephen J. Livingstone[3], Gong Cheng[4], Liming Jiang[1,2], Tom Chudley[5], Brice Noël[6], and Daan Li[7]

[1]State Key Laboratory of Precision Geodesy, Innovation Academy for Precision Measurement Science and Technology, Chinese Academy of Sciences, Wuhan, China, [2]College of Earth and Planetary Science, University of Chinese Academy of Sciences, Beijing, China, [3]Department of Geography, University of Sheffield, Sheffield, UK, [4]Department of Earth Sciences, Dartmouth College, Hanover, NH, USA, [5]Department of Geography, Durham University, Durham, UK, [6]Laboratoire de Climatologie et Topoclimatologie, University of Liège, Liège, Belgium, [7]College of Urban and Environmental Sciences, Yancheng Teachers University, Yancheng, China

Abstract Acceleration of Sermeq Kujalleq has been linked to the retreat of its calving front. However, models consistently underestimate its ice-flow variability, indicating that important physical processes might be ignored, which introduces uncertainties in projecting its future mass loss and sea-level rise contribution. Using the Ice-sheet and Sea-level System Model, we simulate Sermeq Kujalleq from 2016 to 2022 constrained by sub-monthly ice front positions. Changes in front position explain >76% of the velocity variations but with a spatially and seasonally varying misfit between modeled and observed velocities up to 30 km upstream. This misfit significantly correlates with variations in height above flotation within 10 km of the terminus. Incorporating these variations into the model by scaling the basal shear stress reduces the average misfit by over 90%. This indicates that seasonal variations in ice thickness-induced effective pressure and basal conditions play a crucial role in controlling intra-annual and longer-term ice-flow variations.

Plain Language Summary Modeling Sermeq Kujalleq (Jakobshavn Isbræ), the world's fastest marine-terminating glacier, has been a challenge due to a lack of understanding of the key controls governing ice flow. This uncertainty has led to underestimates of its future contribution to sea level rise. To identify driving mechanisms and reduce this uncertainty, we used advanced ice flow model and sub-monthly observations, finding that fluctuations in ice front position accounted for >76% of ice velocity variations up to 30 km upstream. However, there was also a significant seasonal misfit between the modeled and observed speeds, especially in recent years, with the model typically underestimating observed ice flow in late summer and autumn when it is thinner and closer to floating. When variations in the degree of floatation are added to the model the misfit is reduced by over 90%, indicating the crucial role of seasonal ice thickness variation in determining long-term ice flow variations.

Key Points:

- An ice model constrained by observed ice front positions explains >76% of speed variation at Sermeq Kujalleq, independent of friction law
- The misfit with velocity observation extends 30 km upstream and varies seasonally, peaking when the near-terminus region is less grounded
- Variations in effective pressure and basal conditions account for >90% of the velocity misfit during 2016–2022 near the terminus

Supporting Information:

Supporting Information may be found in the online version of this article.

Correspondence to:

L. Jiang,
jlm@whigg.ac.cn

Citation:

Lu, X., Sole, A., Livingstone, S. J., Cheng, G., Jiang, L., Chudley, T., et al. (2025). Ice thickness-induced variations in effective pressure and basal conditions influence seasonal and multi-annual ice velocity at Sermeq Kujalleq (Jakobshavn Isbræ). *Geophysical Research Letters*, *52*, e2024GL111092. https://doi.org/10.1029/2024GL111092

Received 4 JUL 2024
Accepted 19 JAN 2025

Author Contributions:

Conceptualization: Xi Lu, Andrew Sole, Stephen J. Livingstone, Gong Cheng, Liming Jiang
Data curation: Xi Lu, Tom Chudley, Brice Noël
Formal analysis: Xi Lu
Funding acquisition: Liming Jiang
Investigation: Xi Lu
Methodology: Xi Lu, Andrew Sole, Stephen J. Livingstone, Gong Cheng
Resources: Andrew Sole, Stephen J. Livingstone
Software: Gong Cheng
Supervision: Andrew Sole, Stephen J. Livingstone, Liming Jiang

1. Introduction

The Greenland Ice Sheet (GrIS) discharges ice to the ocean through hundreds of marine-terminating glaciers (Mouginot et al., 2019; Wood et al., 2021). Observations and numerical modeling indicate that the retreat and acceleration of these glaciers have been primary drivers of GrIS mass loss, accounting for 66% ± 8% of the total loss and contributing a cumulative 9.1 mm sea level rise equivalent since the late 20th century (Choi et al., 2021; King et al., 2020; Mouginot et al., 2019). Consequently, understanding the mechanisms governing marine-terminating glacier behavior and parameterizing these mechanisms in ice flow models is critical for assessing the present and future state of the GrIS (Enderlin et al., 2014; Straneo & Heimbach, 2013).

Sermeq Kujalleq (Jakobshavn Isbræ) is the fastest flowing marine-terminating glacier and the largest single source of sea-level-rise from the GrIS, losing approximately 250 Gt from 2011 to 2020 (Joughin et al., 2020; Khan et al., 2022; Khazendar et al., 2019). Over the past 2 decades, it has generally exhibited multi-annual retreat, frontal thinning, and widespread acceleration, with a brief phase of re-advance, slowing, and thickening from 2016 to 2019 (Cassotto et al., 2017; Joughin et al., 2020; Khazendar et al., 2019; Lemos et al., 2018). Numerical

Validation: Xi Lu
Visualization: Xi Lu
Writing – original draft: Xi Lu
Writing – review & editing: Andrew Sole, Stephen J. Livingstone, Gong Cheng, Liming Jiang, Tom Chudley, Brice Noël, Daan Li

models suggest that 80%–90% of the upstream acceleration (~40 km upstream along its flowline (Figure 1)) of Sermeq Kujalleq (SK) can be directly attributed to ice-front retreat, triggered by ocean warming and a reduction in the extent and duration of the rigid ice mélange (Cassotto et al., 2019; Joughin et al., 2020; Rosenau et al., 2013; Vieli & Nick, 2011). These changes alter the near-terminus stress regime, driving ice-front retreat and decreasing ice viscosity at the shear margins through stress perturbations (Bondzio et al., 2016, 2017). Near the terminus, SK exhibits high amplitude seasonal variations in ice velocity (Lemos et al., 2018), which are thought to influence the long-term dynamics and overall stability of SK (Cassotto et al., 2019; Joughin et al., 2012; Podrasky et al., 2012). Modeling studies of SK reveal seasonal velocity deviations of up to 40% near the terminus compared to observations, which cannot be fully captured by ice front forcing alone (Bondzio et al., 2017).

Previous studies on other tidewater glaciers in Greenland indicate that the choice of friction law can have a significant impact on the modeled ice velocity (Åkesson et al., 2021; Brondex et al., 2017; Helanow et al., 2021; Zoet & Iverson, 2020). For example, Åkesson et al. (2021) found that simulated ice velocities near the grounding line of Petermann Glacier differed from observations by −7% to 14%, depending on the friction law employed. In contrast, Cheng et al. (2022) and Lippert et al. (2024) revealed that the dynamics of Helheim and Kangerlussuaq Glacier are primarily ice front-driven, independent of the friction law applied. However, it remains unclear which friction law is most appropriate for SK and whether this selection is related to observed velocity deviations. Additionally, seasonal dynamic thinning of SK could lower basal effective pressure by reducing the ice overburden, cause the terminus to approach flotation, reduce basal coupling and enhance ice flow (Cassotto et al., 2019). The rapid supply of meltwater to the ice-bed interface can increase subglacial water pressure, temporarily enhancing basal sliding (Cavanagh et al., 2017). Whether such physical processes contribute to SK's velocity deviations, however, remains unclear.

This study aims to improve understanding of the mechanisms driving seasonal ice dynamic variations at SK and their parameterizations to enhance ice modeling. We follow the approach of prior studies (Bondzio et al., 2017; Cheng et al., 2022; Lippert et al., 2024), using the Ice-sheet and Sea-level System Model (ISSM) (Larour et al., 2012) to simulate the dynamics of SK from 2016 to 2022, driven by sub-monthly observed ice front positions. This approach allows us to isolate the dynamics controlled by the moving ice front, and evaluate the remaining processes to determine the importance and contribution of other drivers.

2. Data and Methods

2.1. Climate Model Data

We used daily surface mass balance (SMB) and runoff outputs from the RACMO2.3p2 regional climate model at 5.5 km resolution from 2016 to 2022, statistically downscaled to 1 km spatial resolution (Noël et al., 2019). SMB data served as realistic climate forcing for the ice flow model. Time series data representing the daily cumulative catchment-integrated runoff from the 1 km resolution drainage basin of SK, as delineated by Mankoff et al. (2020), were utilized for comparison against the ice flow model outputs.

2.2. Observed Ice Front Positions and Surface Ice Velocity

We digitised variable-resolution front positions from Landsat-7/8, Sentinel-1 and Sentinel-2 satellite imagery using the Google Earth Engine Digitization Tool (GEEDiT; Lea, 2018), generating 191 fronts (Figure 1b) from 2016 to 2022. All fronts were converted into a signed distance function, facilitating their integration into transient model simulations at defined time steps (Cheng et al., 2022).

The velocity data from 2016 to 2022 were extracted from the Program for Monitoring of the Greenland Ice Sheet (PROMICE) and the Greenland Climate Network (GC-Net). This data set comprises a 200-m resolution ice-sheet-wide velocity product obtained through Synthetic Aperture Radar (SAR) offset tracking between successive passes captured by the Sentinel-1 satellite (Solgaard et al., 2021).

2.3. Ice Sheet Model Setup and Experiments

We used the Shelfy-Stream Approximation (SSA) implemented in the ISSM to model the dynamics of SK from 2016 to 2022. Although this approach disregards vertical shear, it provides an effective simulation of the ice dynamics at the fast-flowing SK glacier, where basal sliding is the predominant ice flow mechanism (Bondzio et al., 2017; Joughin et al., 2012). The model domain (Figure 1a) encompasses the ice-covered region within the

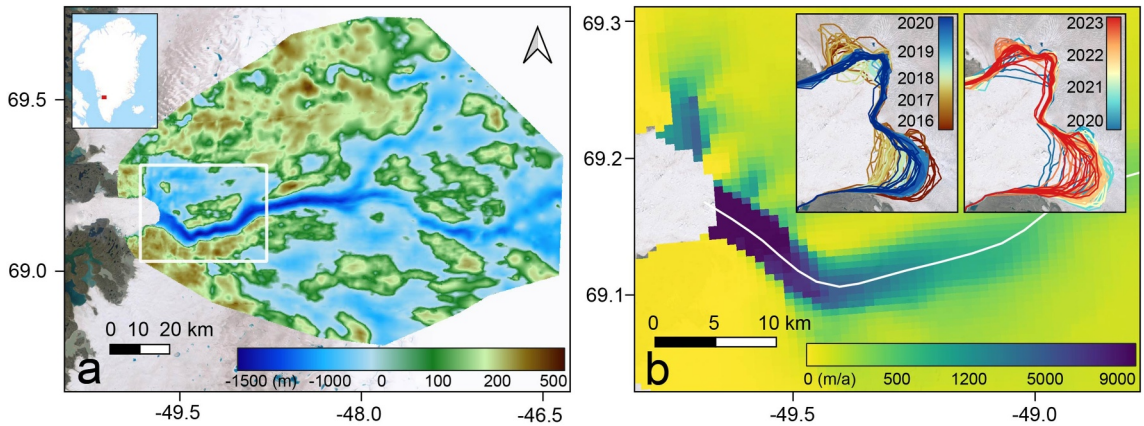

Figure 1. Overview of Sermeq Kujalleq. (a) Bed topography of the model domain (Morlighem et al., 2017, 2022). Background image is from Esri satellite imagery ©Esri. The white box denotes the region of (b). (b) Error-weighted average ice velocity from 2016 to 2022 PROMICE velocity with 200 m resolution (Solgaard et al., 2021) used for inferring the initial basal friction coefficients. The white line denotes the central flow line. Insets show a zoomed-in view of the glacier fronts indicated by colored lines with the color scale in 2019 is expanded compared to others for displaying the denser ice fronts and avoiding shading.

SK catchment flowing faster than 100 m/a. Its northern and southern boundaries align with the catchment outlined by Mankoff et al. (2020).

We used a two-dimensional unstructured triangular mesh, spanning from 100 m resolution in the fast-flowing region to 1,500 m in the interior of the domain. The bed topography and ice mask were sourced from BedMachine Greenland v5 (Morlighem et al., 2017, 2022), which has a grid resolution of 150 m. The initial ice surface elevation was from the ArcticDEM 32 m mosaic (Porter et al., 2023) extracted using pDEMtools (Chudley & Howat, 2024). We used depth-averaged temperature data provided by the ISSM contribution within the ISMIP6 project (Goelzer et al., 2018) to derive a spatially varying rheology parameter for Glen's flow law (Glen, 1958) with a power-law exponent of $n = 3$. The temperature-dependent relationship was derived from Cuffey and Paterson (2010, p. 75). For observed surface velocity used in calibrating the friction coefficients, we employed error-weighted average ice velocity derived from 200 m PROMICE velocity data from 2016 to 2022 (Figures S1–S3 in Supporting Information S1). Following Cheng et al. (2022), we inferred the basal friction coefficient (C) by solving the inverse problem (Morlighem et al., 2010), which minimizes a cost function quantifying the misfit between modeled and observed ice velocities (Text S1 in Supporting Information S1).

We considered three widely recognized friction laws–from an explicit dependence on basal effective pressure (N) over the whole domain for Budd's Law (Equation 1) (Budd et al., 1979) to limited dependence on N for Schoof & Gagliardini's Law (Equation 2) (Schoof, 2005), and no explicit dependence on N for Weertman's Law (Equation 3) (Weertman, 1957):

$$\tau_b = -C_b N |\boldsymbol{v}_b|^{m-1} \boldsymbol{v}_b \tag{1}$$

$$\tau_b = \frac{-C_s |v_b|^{m-1} v_b}{\left(1 + |v_b| \left(\frac{C_s}{C_{\max} N}\right)^{\frac{1}{m}}\right)^m} \tag{2}$$

$$\tau_b = -C_w |\boldsymbol{v}_b|^{m-1} \boldsymbol{v}_b \tag{3}$$

where τ_b is the basal shear stress, $\boldsymbol{v}_b$ is the basal velocity and C_b, C_s, and C_w are the corresponding spatially variable friction coefficients. $C_{\max}$ represents an upper limit of the ratio $\frac{\tau_b}{N}$, called Iken's bound (Iken, A. 1981), and was prescribed a value of 0.8 for our experiments. m are positive constants and take different values (Table S1 in Supporting Information S1). For each friction law, we conducted an inversion to determine the basal friction coefficient and the parameters used for each law are shown in Table S1 of Supporting Information S1. The friction coefficient is fixed through time in all the simulations.

We constrained the model using several-day to monthly observed ice front positions to conduct the transient simulation from 2016 to 2022 at a time step of 1.825 days. Additionally, we conducted a control run for all three friction laws where the ice front position remained fixed at its initial location.

2.4. Height Above Flotation

Height above floatation (H_{af}) can be a proxy for the grounded state of the ice and the effective pressure N based on the assumption that subglacial water has an easy connection to the ocean (Stearns & van der Veen, 2018; Wild et al., 2022). Drawing on this idea, to analyze differences in the spatial and temporal difference between observed velocity and model output, we calculated an approximate H_{af}^{model} using modeled ice surface elevation (s^{model}) and H_{af}^{obs} using monthly CryoSat-2 data (Helm et al., 2014) of ice surface elevation (s^{obs}) from January 2016 to December 2022 along the central flowline shown in Figure 1 as:

$$\mathrm{H}_{af}^{(.)} = \mathrm{s}^{(.)} - \mathrm{h}_f \tag{4}$$

where h_f is theoretical floatation height (Wood et al., 2021).This approximate $H_{af}^{(.)}$ allows for negative values, which occur if h_f exceeds $s^{(.)}$. h_f was estimated using bed elevation data from BedMachine v5 (Figure S4a in Supporting Information S1) (Morlighem et al., 2017, 2022) as:

$$h_f = -b \times \frac{\rho_w - \rho_i}{\rho_i} \tag{5}$$

where b is the bed elevation, and ρ_w and ρ_i, are the densities of ice and ocean water (assigned 910 and 1,028 kg m^{-3}), respectively.

3. Results

3.1. Consistent Transient Behavior From Different Friction Laws

Modeled ice velocities from the three different friction laws closely reproduce observations (Figures 2a–2d), including both interannual and seasonal variations. During the melt season, as SK retreats, all three models exhibit accelerations that propagate upstream. This is followed by deceleration during advance of the ice front in autumn and winter. Since 2020, the seasonal acceleration of ice flow has increased compared to the previous 4 years. Modeled ice flow velocity in the control experiments exhibits no multi-annual or seasonal variation but can reproduce observed ice velocity upstream of 30 km for each friction law considered (Figures 2e, 2i2k, Figures S5 and S6 in Supporting Information S1).

3.2. Spatial and Temporal Patterns of Misfit Between Simulated and Observed Ice Velocity

The introduction of ice-front forcing reduces the mean differences between the control run and observations by ~72.5% (45%–100%) within 0–10 km, and by ~70% (40%–100%) within 10–20 km of the terminus in April (Figure S6 in Supporting Information S1). In September, the differences were reduced by ~56% (13%–100%) within 0–10 km and ~70.5% (41%–100%) within 10–20 km after incorporating ice fronts. Since 2019, modeled velocities forced by ice fronts were 25%–32% slower than observations in late summer within 0–10 km of the terminus (Figure S6 in Supporting Information S1). Upstream of 30 km, the control run can accurately reproduce up to 100% of the observed velocities before and after the melt season (April and September) (Figure S6 in Supporting Information S1).

We extracted average velocities along the central flow line at 0–10 km, 10–20 km, and 30–40 km from the terminus (Figures 2i–2k). Within 10 km of the terminus, modeled ice velocities follow winter and spring observations but are consistently lower in the late- and post-melt season (August to December) of each year (Figure 2i). In 2016, the modeled velocity was ~14% below the observed velocity in the post-melt season (Figure S7 in Supporting Information S1). In 2017, the misfit appeared after August 26, peaking on November 5 at about 1,439 m/a, with the model being ~14% slower than observations. Compared to previous years, there was a notable reduction in the difference between modeled and observed velocities in 2018. In 2019, the misfit started on August 25, reaching its peak at about 1,946 m/a on October 26, with the model being ~18% slower than

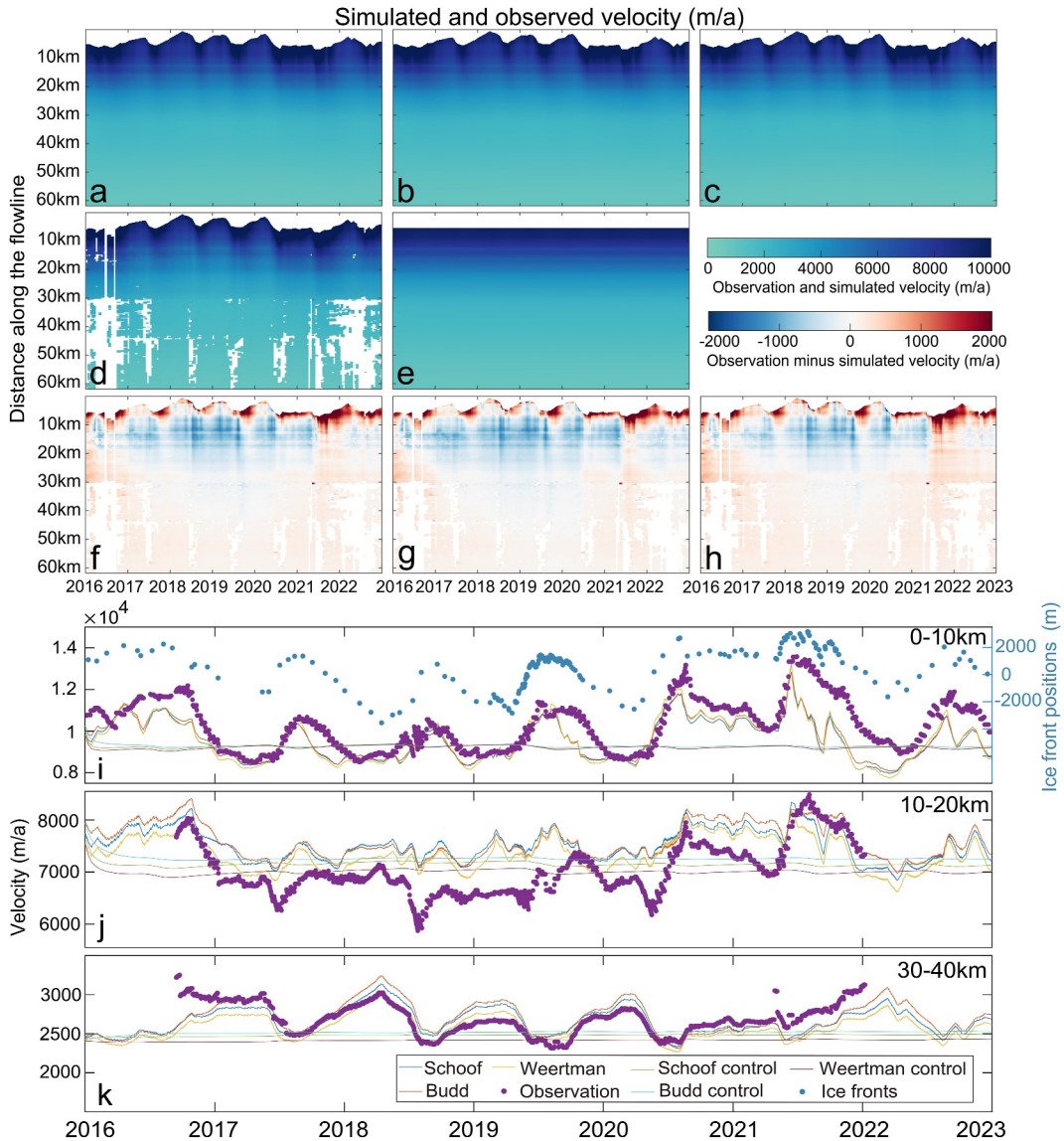

Figure 2. Ice velocity extracted along the central flow line from 2016 to 2022. (a–c) Schoof, Budd and Weertman friction law experiments. (d) Observation. (e) Control run using a fixed ice front position and Budd's law. The control experiments for other laws are shown in Figure S5 of Supporting Information S1. (f–h) Comparison between model output (Schoof, Budd and Weertman, respectively) and observation. (i–k) Spatially averaged ice velocity in the segments: 0–10, 10–20, and 30–40 km, from the ice front. Blue dots in penal (i) show observed ice front positions relative to the latest front.

observations. The misfit in 2020 initiated on August 13, with its peak of ∼2186 m/a (model ∼17% slower than observations) on August 21. Since 2021, the end-of-melt-season misfit increased sharply, starting on June 17 and peaking on August 28 with an average misfit of ∼3,278 m/a within 0–10 km. During this period, modeled ice velocity was 26% slower than observations, with differences exceeding 5,000 m/a within 1 km from the ice front.

Between 10 and 20 km from the terminus, modeled ice velocity is typically 10%–20% faster than observations, with some larger spikes in 2017, 2018 and 2020 of up to 22% (Figure 2j, Figure S7 in Supporting Information S1), typically during the early melt season. The misfit persists throughout 2017–2021 until model velocities match observations in the melt season of 2021. Upstream of 30 km, observed and modeled ice velocities match well, with misfits typically <8% (Figure 2k, Figure S7 in Supporting Information S1).

4. Discussion

Over 76% of the spatiotemporal variation of SK's velocity can be attributed to fluctuations in ice front position. This is consistent with an earlier modeling study of SK between 1985 and 2016 (Bondzio et al., 2017) demonstrating that recession of the ice front induces widespread inland acceleration and thinning by reducing lateral drag and transmitting stress perturbations inland along deep troughs with low basal drag (Nick et al., 2009). In the control experiments with a fixed ice front, the modeled velocity diverges from observations close to the terminus but matches from ∼30 km upstream (Figure S6 in Supporting Information S1). This 30 km limit coincides with a steep bed knickpoint (Figure S4b in Supporting Information S1), which might have limited the continued upstream propagation of direct and diffusive terminus-controlled effects (Felikson et al., 2021).

Although ice-front positions can explain over 76% of the velocity variations, a distinct seasonally varying misfit persists across both data sets used for inversion and ice-front position, and across all friction inversions. This misfit is largest close to the terminus in 2021, indicating that other processes may also influence seasonal velocity variations (Joughin et al., 2012). Here, we seek to explain the remaining misfit, by evaluating the choice of friction law, variations in H_{af} and meltwater delivery to the ice bed.

4.1. Choice of Friction Law

The friction coefficient C implicitly accounts for bed properties, such as roughness and substrate (Joughin et al., 2019). In our transient simulations, the functional dependence of basal stress τ_b on bed conditions is represented through C (Gillet-Chaulet et al., 2016), which is calculated using a "snapshot" inversion approach for different friction laws. Thus, the model neglects the dependence between τ_b and evolving bed conditions (Bondzio et al., 2017; Khan et al., 2022; McArthur et al., 2023).

Block and Bell (2011) demonstrate that soft sediments exist in the main trough of SK up to 40 km from the terminus, with a thickness of 500–1,000 m within 0–10 km along the centerline in Figure 1a. These low shear strength sediments fill topographic lows, effectively smoothing basal irregularities, providing limited resistance to ice flow (Maier et al., 2021). Habermann et al. (2013) demonstrated the decrease in effective pressure N caused a temporal weakening of basal yield stress of till near the terminus area of SK based on several inversions (Tulaczyk et al., 2000). In other words, seasonal dynamic thinning, driven by the significant retreat of the ice front and increased surface melt, could induce SK to accelerate by weakening the bed. This process reduces interparticle contact forces and friction, alters the basal conditions, and ultimately accelerates glacier sliding (Shapero et al., 2016; Stearns & van der Veen, 2018; Walter et al., 2014). Thus, the velocity misfit observed could potentially stem from using a time-fixed basal friction based on a snapshot inversion, leading the models to underestimate ice flow velocity in the late melt season and show the net ice displacement over longer periods.

In addition, the effective pressure N varies temporally in Budd's and Schoof's laws but is not explicitly accounted for in Weertman's law. However, our three friction-law model outputs consistently simulated similar ice velocity fields and velocity misfit. This suggests the temporal variation of N considered by Schoof's and Budd's friction laws are not able to fully capture the dynamics driven by this variability. To confirm if the variation of N is well reproduced by the model, we calculated the relative variation of $H_{af}{}^{\text{model}}$ compared to the initial state $H_{af}{}^{0}$ (Figure 3a), as a proxy for N (Stearns & van der Veen, 2018; Wild et al., 2022), and compared this with the relative variation of $H_{af}{}^{\text{obs}}$ (Figure 3b, Figure S8a in Supporting Information S1).

Figure 3b shows a significant seasonal difference in H_{af} between the model and observations within 0–10 km of the terminus. For example, the model captured approaching flotation during the melt season in 2020 (−32.2 m from observation vs. −55.1 m from the model), but the grounding state before and after the melt season differs significantly from observations (127.7 m vs. −15.4 m, −2.5 m vs. −57.3 m) within 0–10 km of the terminus. A similar pattern was observed in 2021. This inability of the models to capture the grounding state variation indicates a deficiency in representing seasonal dynamic thinning, and restabilization as the thick ice advects toward the terminus within the model (Cassotto et al., 2019). Joughin et al. (2012) demonstrated that thinning-induced changes in N primarily influence SK 8–10 km upstream from the grounding line. We propose that inaccurately reproducing seasonal ice thickness variations in the model could contribute a component of the seasonal near-terminus velocity deviation.

10.1029/2024GL111092

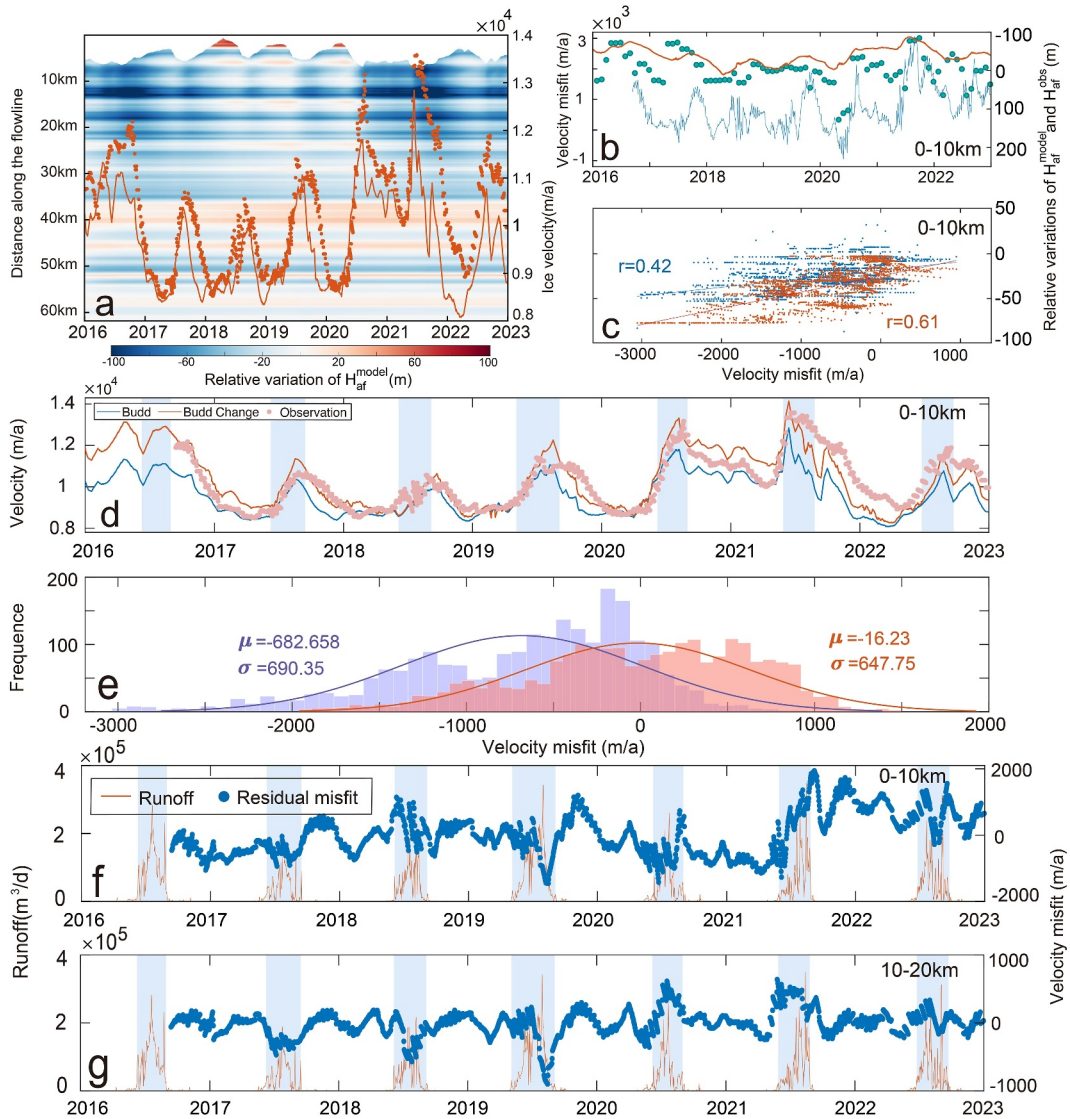

Figure 3. (a) Comparison of H_{af} variation and ice velocity, with modeled (orange line) and observed (points) velocities within 0–10 km. (b) Velocity misfit (blue line) and H_{af}^{model} (orange line) and H_{af}^{obs} (turquoise points). (c) Correlation of velocity misfit with $H_{af}^{(.)}$ variation: $r^2 = 0.26$ ($p < 0.0001$) for H_{af}^{obs} (blue points) and $r^2 = 0.37$ ($p < 0.0001$) for H_{af}^{model} (orange points). (d). Comparison of observed and modeled ice velocities before and after introducing H_{af}^{model} variation. (e) Misfit distribution between modeled and observed velocities before (violet) and after (red) adjusting basal shear stress. (f–g) Runoff variation and melt season (light-blue bars). Residual velocity misfit after incorporating H_{af}^{model} variation and removing trends within 10–20 km.

4.2. Increased Near-Terminus Misfit When the Glacier Is Less Grounded

We found a synchronisation and significant linear correlation between $H_{af}^{(.)}$ variation and the near-terminus velocity misfit using both observations and modeled outputs within 0–10 km of the terminus (observation: $r = 0.42$; model: $r = 0.61$, $P < 0.0001$) (Figures 3a–3c). Figure 3a shows the similar observed seasonal patterns of increased flotation and increased observed-minus-modeled velocity misfit near the terminus.

For further validation and to reduce the velocity misfit, we incorporated variations in the basal condition to enhance its seasonality and adjusted basal shear stress using H_{af}^{obs} and H_{af}^{model} (Figure 3d, Figure S10 in Supporting Information S1). Basal shear stress was scaled by the ratio of $H_{af}^{(.)}$ to its initial state H_{af}^{0} only within

0–10 km (Text S3 in Supporting Information S1). An example set of modeled velocity maps from August 2021 is provided in Figure S9 of Supporting Information S1. Taking Budd's law as an example, this scaling produced an over 90% reduction in observed-modeled ice velocity misfit within 0–10 km of the terminus (Figures 3d and 3e), supporting ice thickness-induced seasonal changes in basal shear stress as the causes of velocity misfit in the late melt season, and indicating that up to 22% of SK's acceleration in the late melt season can be explained by seasonal fluctuations in basal conditions. One possible explanation is that during ice front retreat and dynamic thinning, the effective pressure decreases and the near-terminus region approaches flotation, which weakens basal coupling, makes the sediment more prone to deformation, changes the basal friction and accelerates ice flow (Cassotto et al., 2019; Habermann et al., 2013). The variation of H_{af} as a proxy for N and bed conditions changes can be used as a simple approach to better parameterize ice-flow close to the terminus of a marine-terminating glacier, like a pseudoplastic friction power law (Åkesson et al., 2021). Nevertheless, it is important to note that within the current modeling framework, we are unable to fully disentangle the variations between effective pressure and friction coefficients.

4.3. Seasonal Response to Meltwater Inputs

Large, transient increases in basal water delivery can increase subglacial water pressure and decrease N, leading to rapid, short-lived glacier dynamics (Andersen et al., 2017; Davison et al., 2020; Podrasky et al., 2012; Schoof, 2010). However, the velocity misfit lasted significantly longer than the melt season, and runoff magnitude does not correspond to velocity misfit on a multi-year scale, suggesting meltwater inputs are not the main cause (Habermann et al., 2013; Joughin et al., 2004, 2008). For example, despite the lower runoff peak in 2018 (2.2×10^5 m³/d) compared to 2019 (3.4×10^5 m³/d) (Figures 3f and 3g), the velocity misfits are similar. In contrast, while runoff peaks in 2019 and 2021 (3.4×10^5 and 3.5×10^5 m³/d) are nearly identical, the velocity misfit is greater in 2021.

After accounting for N and basal friction variations induced by dynamic thinning (variation in H_{af}^{model}) within 0–10 km of the terminus and removing long-term trends from the modeled velocity within 10–20 km, we identified low excursions in the residual misfit during periods of high runoff (Figures 3f and 3g). For example, in 2018–2019, during the initial runoff increase, the residual misfit briefly rises within the 0–10 km and 10–20 km domain, where surface crevasses, as indicated by observations, allow runoff to reach the ice bed (Lampkin et al., 2013). This could result from lower N due to increased subglacial water pressure. The residual misfit then decreases rapidly before rising again (toward zero) after the runoff peak. This change may indicate the development of hydraulically efficient subglacial channels, which increase N (Davison et al., 2020; Schoof, 2010). Overall, the impact of runoff on SK's velocity is limited to less than 10%, and on a seasonal time scale, quickly recovering after surface melt ceases.

5. Conclusions

This study provides a comprehensive modeling analysis of the seasonal and inter-annual ice flow variability of Sermeq Kujalleq (Jakobshavn Isbræ) from 2016 to 2022. The model reproduces approximately 76% of the observed velocity variability when forced with observed sub-monthly ice front positions. We identify a misfit between modeled and observed ice velocity within 0–10 km from the terminus, which is significantly correlated with the variations in the "height above flotation", H_{af}. As a proxy for fluctuations in effective pressure and the main driver of reduced basal yield stress, we incorporated H_{af} variations into the model, explaining over 90% of the misfit within 0–10 km of the terminus. Variations in surface runoff coincide with troughs in the residual misfit after considering transient basal friction variation and ice thickness-induced effective pressure, indicating a short-term and less than 10% influence of surface melt-driven variations on ice velocity. We conclude that while ice front position is the primary driver of Sermeq Kujalleq's velocity variability, seasonal variations in effective pressure and basal conditions driven by dynamic thinning and subglacial hydrology significantly affect its interannual and seasonal acceleration, which responsible for the observed-modeled velocity misfit. As Sermeq Kujalleq continues to retreat into a deeper basin, it will likely remain sensitive to seasonal variations in effective pressure. These findings underscore the importance of incorporating seasonal fluctuations in effective pressure and variable basal conditions into ice dynamic simulations. Accurately parameterizing these factors is crucial for improving projections of both the timing and magnitude of glacier retreat.

Data Availability Statement

Ice bed data is from BedMachine Greenland v5 (Morlighem et al., 2022). Ice velocity maps are from Solgaard et al. (2021) and were provided by the Geological Survey of Denmark and Greenland (GEUS). CryoSat-2 data is from Helm et al. (2014). ArcticDEM data is available from Porter et al. (2023). ISSM is open source and can be downloaded and installed via ISSM Team. (2023) as either binaries or source code. Results generated during the study are available for download via Xi, L. et al. (2024).

Acknowledgments
This work was funded by the National Key R&D Program of China (Grant 2018YFC1406102 and 2017YFA0603103), the Strategic Priority Research Program of the Chinese Academy of Sciences (Grant XDA19070104), and the National Natural Science Foundation of China (Grant 42174046). We also gratefully acknowledge financial support from China Scholarship Council. BN was funded by the Fonds de la Recherche Scientifique de Belgique (F.R.S.-FNRS). GC acknowledges support from the Novo Nordisk Foundation under the Challenge Programme 2023 (Grant NNF23OC00807040).

References

Åkesson, H., Morlighem, M., O'Regan, M., & Jakobsson, M. (2021). Future projections of Petermann Glacier under ocean warming depend strongly on friction law. *Journal of Geophysical Research: Earth Surface*, *126*(6), e2020JF005921. https://doi.org/10.1029/2020JF005921

Andersen, M. L., Nettles, M., Elosegui, P., Larsen, T. B., Hamilton, G. S., & Stearns, L. A. (2017). Quantitative estimates of velocity sensitivity to surface melt variations at a large Greenland outlet glacier. *Journal of Glaciology*, *57*(204), 609–620. https://doi.org/10.3189/002214311797409785

Block, A. E., & Bell, R. E. (2011). Geophysical evidence for soft bed sliding at Jakobshavn Isbrae, West Greenland. *The Cryosphere Discussions*, *2011*, 339–366. https://doi.org/10.5194/tcd-5-339-2011

Bondzio, J. H., Morlighem, M., Seroussi, H., Kleiner, T., Rückamp, M., Mouginot, J., et al. (2017). The mechanisms behind Jakobshavn Isbrae's acceleration and mass loss: A 3-D thermomechanical model study. *Geophysical Research Letters*, *44*(12), 6252–6260. https://doi.org/10.1002/2017gl073309

Bondzio, J. H., Seroussi, H., Morlighem, M., Kleiner, T., Rückamp, M., Humbert, A., & Larour, E. Y. (2016). Modelling calving front dynamics using a level-set method: Application to Jakobshavn Isbræ, West Greenland. *The Cryosphere*, *10*(2), 497–510. https://doi.org/10.5194/tc-10-497-2016

Brondex, J., Gagliardini, O., Gillet-Chaulet, F., & Durand, G. (2017). Sensitivity of grounding line dynamics to the choice of the friction law. *Journal of Glaciology*, *63*(241), 854–866. https://doi.org/10.1017/jog.2017.51

Budd, W. F., Keage, P. L., & Blundy, N. A. (1979). Empirical studies of ice sliding. *Journal of Glaciology*, *23*(89), 157–170. https://doi.org/10.3189/S0022143000029804

Cassotto, R., Fahnestock, M., Amundson, J. M., Truffer, M., Boettcher, M. S., De La PeÑA, S., & Howat, I. A. N. (2019). Non-linear glacier response to calving events, Jakobshavn Isbræ, Greenland. *Journal of Glaciology*, *65*(249), 39–54. https://doi.org/10.1017/jog.2018.90

Cassotto, R., Fahnestock, M., Amundson, J. M., Truffer, M., & Joughin, I. (2017). Seasonal and interannual variations in ice melange and its impact on terminus stability, Jakobshavn Isbræ, Greenland. *Journal of Glaciology*, *61*(225), 76–88. https://doi.org/10.3189/2015JoG13J235

Cavanagh, J. P., Lampkin, D. J., & Moon, T. (2017). Seasonal variability in regional ice flow due to meltwater injection into the shear margins of Jakobshavn Isbræ. *Journal of Geophysical Research: Earth Surface*, *122*(12), 2488–2505. https://doi.org/10.1002/2016jf004187

Cheng, G., Morlighem, M., Mouginot, J., & Cheng, D. (2022). Helheim Glacier's terminus position controls its seasonal and inter-annual ice flow variability. *Geophysical Research Letters*, *49*(5), e2021GL097085. https://doi.org/10.1029/2021GL097085

Choi, Y., Morlighem, M., Rignot, E., & Wood, M. (2021). Ice dynamics will remain a primary driver of Greenland ice sheet mass loss over the next century. *Communications Earth & Environment*, *2*(1), 26. https://doi.org/10.1038/s43247-021-00092-z

Chudley, T. R., & Howat, I. M. (2024). pDEMtools. In (Version 0.6). https://github.com/trchudley/pDEMtools

Cuffey, K. M., & Paterson, W. S. B. (2010). The physics of glaciers (Ed. 4).

Davison, B. J., Sole, A. J., Cowton, T. R., Lea, J. M., Slater, D. A., Fahrner, D., & Nienow, P. W. (2020). Subglacial drainage evolution modulates seasonal ice flow variability of three tidewater glaciers in southwest Greenland. *Journal of Geophysical Research: Earth Surface*, *125*(9), e2019JF005492. https://doi.org/10.1029/2019jf005492

Enderlin, E. M., Howat, I. M., Jeong, S., Noh, M.-J., van Angelen, J. H., & van den Broeke, M. R. (2014). An improved mass budget for the Greenland ice sheet. *Geophysical Research Letters*, *41*(3), 866–872. https://doi.org/10.1002/2013GL059010

Felikson, D. G. A. C., Bartholomaus, T. C., Morlighem, M., & Noel, B. P. Y. (2021). Steep Glacier bed Knickpoints mitigate inland thinning in Greenland. *Geophysical Research Letters*, *48*(2), e2020GL090112. https://doi.org/10.1029/2020GL090112

Gillet-Chaulet, F., Durand, G., Gagliardini, O., Mosbeux, C., Mouginot, J., Rémy, F., & Ritz, C. (2016). Assimilation of surface velocities acquired between 1996 and 2010 to constrain the form of the basal friction law under Pine Island Glacier. *Geophysical Research Letters*, *43*(19), 310311–310321. https://doi.org/10.1002/2016GL069937

Glen, J. W. (1958). Union Géodésique et Géophysique Internationale. Association Internationale d'Hydrologie Scientifique. Symposium de Chamonix, 16–24 sept. 1958. *Journal of Glaciology*, *3*, 965–978.

Goelzer, H., Nowicki, S., Edwards, T., Beckley, M., Abe-Ouchi, A., Aschwanden, A., et al. (2018). Design and results of the ice sheet model initialisation experiments initMIP-Greenland: An ISMIP6 intercomparison. *The Cryosphere*, *12*(4), 1433–1460. https://doi.org/10.5194/tc-12-1433-2018

Habermann, M., Truffer, M., & Maxwell, D. (2013). Changing basal conditions during the speed-up of Jakobshavn Isbræ, Greenland. *The Cryosphere*, *7*(6), 1679–1692. https://doi.org/10.5194/tc-7-1679-2013

Helanow, C., Iverson, N. R., Woodard, J. B., & Zoet, L. K. (2021). A slip law for hard-bedded glaciers derived from observed bed topography. *Science Advances*, *7*(20), eabe7798. https://doi.org/10.1126/sciadv.abe7798

Helm, V., Humbert, A., & Miller, H. (2014). Elevation and elevation change of Greenland and Antarctica derived from CryoSat-2. *The Cryosphere*, *8*(4), 1539–1559. https://doi.org/10.5194/tc-8-1539-2014

Iken, A. (1981). The effect of the subglacial water pressure on the sliding velocity of a glacier in an idealized case. *Journal of Glaciology*, *27*(97), 407–421. https://doi.org/10.3189/S0022143000011448

ISSM Team. (2023). Ice-sheet and Sea-level System Model source code, v4.23 r27919. *Zenodo*. https://doi.org/10.5281/zenodo.8436924

Joughin, I., Abdalati, W., & Fahnestock, M. (2004). Large fluctuations in speed on Greenland's Jakobshavn Isbræ glacier. *Nature*, *432*(7017), 608–610. https://doi.org/10.1038/nature03130

Joughin, I., Das, S. B., King, M. A., Smith, B. E., Howat, I. M., & Moon, T. (2008). Seasonal speedup along the western flank of the Greenland ice sheet. *Science*, *320*(5877), 781–783. https://doi.org/10.1126/science.1153288

Joughin, I., Shean, D. E., Smith, B. E., & Floricioiu, D. (2020). A decade of variability on Jakobshavn Isbræ: Ocean temperatures pace speed through influence on mélange rigidity. *The Cryosphere*, *14*(1), 211–227. https://doi.org/10.5194/tc-14-211-2020

Joughin, I., Smith, B. E., Howat, I. M., Floricioiu, D., Alley, R. B., Truffer, M., & Fahnestock, M. (2012). Seasonal to decadal scale variations in the surface velocity of Jakobshavn Isbrae, Greenland: Observation and model-based analysis. *Journal of Geophysical Research*, *117*(F2). https://doi.org/10.1029/2011JF002110

Joughin, I., Smith, B. E., & Schoof, C. G. (2019). Regularized coulomb friction laws for ice sheet sliding: Application to pine island glacier, Antarctica. *Geophysical Research Letters*, *46*(9), 4764–4771. https://doi.org/10.1029/2019GL082526

Khan, S. A., Bamber, J. L., Rignot, E., Helm, V., Aschwanden, A., Holland, D. M., et al. (2022). Greenland mass trends from airborne and satellite altimetry during 2011–2020. *Journal of Geophysical Research: Earth Surface*, *127*(4), e2021JF006505. https://doi.org/10.1029/2021JF006505

Khazendar, A., Fenty, I. G., Carroll, D., Gardner, A., Lee, C. M., Fukumori, I., et al. (2019). Interruption of two decades of Jakobshavn Isbrae acceleration and thinning as regional ocean cools. *Nature Geoscience*, *12*(4), 277–283. https://doi.org/10.1038/s41561-019-0329-3

King, M. D., Howat, I. M., Candela, S. G., Noh, M. J., Jeong, S., Noël, B. P. Y., et al. (2020). Dynamic ice loss from the Greenland Ice Sheet driven by sustained glacier retreat. *Communications Earth & Environment*, *1*(1), 1. https://doi.org/10.1038/s43247-020-0001-2

Lampkin, D. J., Amador, N., Parizek, B. R., Farness, K., & Jezek, K. (2013). Drainage from water-filled crevasses along the margins of Jakobshavn Isbræ: A potential catalyst for catchment expansion. *Journal of Geophysical Research: Earth Surface*, *118*(2), 795–813. https://doi.org/10.1002/jgrf.20039

Larour, E., Seroussi, H., Morlighem, M., & Rignot, E. (2012). Continental scale, high order, high spatial resolution, ice sheet modeling using the Ice Sheet System Model (ISSM). *Journal of Geophysical Research*, *117*(F1). https://doi.org/10.1029/2011JF002140

Lea, J. M. (2018). The Google Earth Engine Digitisation Tool (GEEDiT) and the Margin change Quantification Tool (MaQiT) – Simple tools for the rapid mapping and quantification of changing Earth surface margins. *Earth Surface Dynamics*, *6*(3), 551–561. https://doi.org/10.5194/esurf-6-551-2018

Lemos, A., Shepherd, A., McMillan, M., Hogg, A. E., Hatton, E., & Joughin, I. (2018). Ice velocity of Jakobshavn Isbræ, Petermann Glacier, Nioghalvfjerdsfjorden, and Zachariæ Isstrøm, 2015–2017, from Sentinel 1-a/b SAR imagery. *The Cryosphere*, *12*(6), 2087–2097. https://doi.org/10.5194/tc-12-2087-2018

Lippert, E. Y. H., Morlighem, M., Cheng, G., & Khan, S. A. (2024). Modeling a century of change: Kangerlussuaq Glacier's mass loss from 1933 to 2021. *Geophysical Research Letters*, *51*(4), e2023GL106286. https://doi.org/10.1029/2023GL106286

Maier, N., Gimbert, F., Gillet-Chaulet, F., & Gilbert, A. (2021). Basal traction mainly dictated by hard-bed physics over grounded regions of Greenland. *The Cryosphere*, *15*(3), 1435–1451. https://doi.org/10.5194/tc-15-1435-2021

Mankoff, K. D., Noël, B., Fettweis, X., Ahlstrøm, A. P., Colgan, W., Kondo, K., et al. (2020). Greenland liquid water discharge from 1958 through 2019. *Earth System Science Data*, *12*(4), 2811–2841. https://doi.org/10.5194/essd-12-2811-2020

McArthur, K., McCormack, F. S., & Dow, C. F. (2023). Basal conditions of Denman Glacier from glacier hydrology and ice dynamics modeling. *The Cryosphere*, *17*(11), 4705–4727. https://doi.org/10.5194/tc-17-4705-2023

Morlighem, M., Rignot, E., Seroussi, H., Larour, E., Ben Dhia, H., & Aubry, D. (2010). Spatial patterns of basal drag inferred using control methods from a full-Stokes and simpler models for Pine Island Glacier, West Antarctica. *Geophysical Research Letters*, *37*(14). https://doi.org/10.1029/2010gl043853

Morlighem, M., Williams, C. N., Rignot, E., An, L., Arndt, J. E., Bamber, J. L., et al. (2022). *IceBridge BedMachine Greenland version 5 NASA national snow and ice data center*. Distributed Active Archive Center. https://doi.org/10.5067/GMEVBWFLWA7X

Morlighem, M., Williams, C. N., Rignot, E., An, L., Arndt, J. E., Bamber, J. L., et al. (2017). BedMachine v3: Complete bed topography and ocean bathymetry mapping of Greenland from multibeam echo sounding combined with mass conservation. *Geophysical Research Letters*, *44*(21), 11051–011061. https://doi.org/10.1002/2017GL074954

Mouginot, J., Rignot, E., Bjork, A. A., van den Broeke, M., Millan, R., Morlighem, M., et al. (2019). Forty-six years of Greenland Ice Sheet mass balance from 1972 to 2018. *Proceedings of the National Academy of Sciences of the U S A*, *116*(19), 9239–9244. https://doi.org/10.1073/pnas.1904242116

Nick, F. M., Vieli, A., Howat, I. M., & Joughin, I. (2009). Large-scale changes in Greenland outlet glacier dynamics triggered at the terminus. *Nature Geoscience*, *2*(2), 110–114. https://doi.org/10.1038/ngeo394

Noël, B., van de Berg, W. J., Lhermitte, S., & van den Broeke, M. R. (2019). Rapid ablation zone expansion amplifies north Greenland mass loss. *Science Advances*, *5*(9), eaaw0123. https://doi.org/10.1126/sciadv.aaw0123

Podrasky, D., Truffer, M., Fahnestock, M., Amundson, J. M., Cassotto, R., & Joughin, I. (2012). Outlet glacier response to forcing over hourly to interannual timescales, Jakobshavn Isbræ, Greenland. *Journal of Glaciology*, *58*(212), 1212–1226. https://doi.org/10.3189/2012JoG12J065

Porter, C., Howat, I., Noh, M.-J., Husby, E., Khuvis, S., Danish, E., et al. (2023). ArcticDEM—mosaics, version 4.1 version V1) [digital elevation model]. *Harvard Dataverse*. https://doi.org/10.7910/DVN/3VDC4W

Rosenau, R., Schwalbe, E., Maas, H.-G., Baessler, M., & Dietrich, R. (2013). Grounding line migration and high-resolution calving dynamics of Jakobshavn Isbræ, West Greenland. *Journal of Geophysical Research: Earth Surface*, *118*(2), 382–395. https://doi.org/10.1029/2012JF002515

Schoof, C. (2005). The effect of cavitation on glacier sliding. *Proceedings of the Royal Society A: Mathematical, Physical and Engineering Sciences*, *461*(2055), 609–627. https://doi.org/10.1098/rspa.2004.1350

Schoof, C. (2010). Ice-sheet acceleration driven by melt supply variability. *Nature*, *468*(7325), 803–806. https://doi.org/10.1038/nature09618

Shapero, D. R., Joughin, I. R., Poinar, K., Morlighem, M., & Gillet-Chaulet, F. (2016). Basal resistance for three of the largest Greenland outlet glaciers. *Journal of Geophysical Research-Earth Surface*, *121*(1), 168–180. https://doi.org/10.1002/2015jf003643

Solgaard, A., Kusk, A., Merryman Boncori, J. P., Dall, J., Mankoff, K. D., Ahlstrøm, A. P., et al. (2021). Greenland ice velocity maps from the PROMICE project. *Earth System Science Data*, *13*(7), 3491–3512. https://doi.org/10.5194/essd-13-3491-2021

Stearns, L. A., & van der Veen, C. J. (2018). Friction at the bed does not control fast glacier flow. *Science*, *361*(6399), 273–277. https://doi.org/10.1126/science.aat2217

Straneo, F., & Heimbach, P. (2013). North Atlantic warming and the retreat of Greenland's outlet glaciers. *Nature*, *504*(7478), 36–43. https://doi.org/10.1038/nature12854

Tulaczyk, S., Kamb, W. B., & Engelhardt, H. F. (2000). Basal mechanics of ice stream B, west Antarctica: 1. Till mechanics. *Journal of Geophysical Research*, *105*(B1), 463–481. https://doi.org/10.1029/1999JB900329

Vieli, A., & Nick, F. M. (2011). Understanding and modelling rapid dynamic changes of tidewater outlet glaciers: Issues and implications. *Surveys in Geophysics*, *32*(4), 437–458. https://doi.org/10.1007/s10712-011-9132-4

Walter, F., Chaput, J., & Lüthi, M. P. (2014). Thick sediments beneath Greenland's ablation zone and their potential role in future ice sheet dynamics. *Geology*, *42*(6), 487–490. https://doi.org/10.1130/g35492.1

Weertman, J. (1957). On the sliding of glaciers. *Journal of Glaciology*, *3*(21), 33–38. https://doi.org/10.3189/S0022143000024709

Wild, C. T., Alley, K. E., Muto, A., Truffer, M., Scambos, T. A., & Pettit, E. C. (2022). Weakening of the pinning point buttressing Thwaites glacier, West Antarctica. *The Cryosphere*, *16*(2), 397–417. https://doi.org/10.5194/tc-16-397-2022

Wood, M., Rignot, E., Fenty, I., An, L., Bjork, A., van den Broeke, M., et al. (2021). Ocean forcing drives glacier retreat in Greenland. *Science Advances*, *7*(1), eaba7282. https://doi.org/10.1126/sciadv.aba7282

Xi, L., Andrew, S., Stephen, J. L., Gong, C., & Liming, J. (2024). Simulating seasonal to inter-annual variability of Sermeq Kujalleq Glacier using ISSM. https://doi.org/10.5281/zenodo.12606538

Zoet, L. K., & Iverson, N. R. (2020). A slip law for glaciers on deformable beds. *Science*, *368*(6486), 76–78. https://doi.org/10.1126/science.aaz1183

References From the Supporting Information

Nuth, C., & Kääb, A. (2011). Co-registration and bias corrections of satellite elevation data sets for quantifying glacier thickness change. *The Cryosphere*, *5*(1), 271–290. https://doi.org/10.5194/tc-5-271-2011